

Structural Dependence of Excitonic Optical Transitions and Band-Gap Energies in Carbon Nanotubes

Gordana Dukovic,^{*,†} Feng Wang,^{‡,§} Daohua Song,[‡] Matthew Y. Sfeir,[†]
Tony F. Heinz,[‡] and Louis E. Brus[†]

*Department of Chemistry, Columbia University, 3000 Broadway,
New York, New York 10027, and Departments of Physics and Electrical Engineering,
Columbia University, 538 West 120th Street, New York, New York 10027*

Received September 8, 2005; Revised Manuscript Received October 4, 2005

ABSTRACT

The optical transitions of semiconducting carbon nanotubes have been ascribed to excitons. Here we use two-photon excitation spectroscopy to measure exciton binding energies, as well as band-gap energies, in a range of individual species of semiconducting SWNTs. Exciton binding energies are large and vary inversely with nanotube diameter, as predicted by theory. Band-gap energies are significantly blue-shifted from values predicted by tight-binding calculations.

Single-walled carbon nanotubes (SWNTs) have remarkable electronic and optical properties arising from reduced dimensionality in a system with strong covalent sp^2 carbon bonds.¹ A Hückel-type tight-binding electronic structure calculation identifies metallic and semiconducting SWNT structures and associates the observed optical transitions with van Hove resonances.¹ However, this analysis does not consider the many-body interactions among the confined carriers, which should be particularly strong in this one-dimensional system.² Ando originally predicted that the many-body interactions would shift the band gaps of semiconducting SWNTs to higher energies and create excitons with significant electron–hole binding energy in the excited electronic state.³ Such strong many-body interactions are supported by further theoretical work^{4–10} and several recent experiments.^{11–14} We have shown experimentally that for a (6,5) SWNT with a diameter of 0.76 nm, the exciton binding energy is roughly 0.42 eV, which is a significant fraction of the band gap.¹² This result suggests that excitonic effects may dominate all aspects of the optical properties of carbon nanotubes: optical absorption, fluorescence, Raman, and Rayleigh scattering of SWNTs.

How does the effect of many-body interactions on the optical properties of carbon nanotubes vary with nanotube structure, i.e., diameter and chirality? In this Letter, we use two-photon excitation spectroscopy to measure exciton

binding and band-gap energies in semiconducting SWNTs as a function of nanotube structure. We show that the exciton binding energy is inversely proportional to nanotube diameter, in agreement with recent theoretical predictions.^{6,7} Within our experimental resolution, we do not observe chiral angle dependence. The measured band-gap energies are significantly higher than those predicted by tight-binding theory.

To investigate structural dependence of excitonic effects, we studied semiconducting SWNTs produced by the HiPCO method^{15,16} in the diameter range of 0.76–1.18 nm. SWNTs were solubilized in aqueous poly(maleic acid/octyl vinyl ether) solution as described elsewhere.¹⁷ To minimize the infrared absorption of water, a drop of this solution was slowly dried to form a film of SWNTs embedded in the polymer matrix. The SWNT fluorescence from the front surface of this film is comparable to the SWNT fluorescence in the parent solution. The fluorescence peak energies are within 2–3 meV of those for SWNTs in SDS solution.¹⁸

In two-photon excitation spectroscopy, we observe SWNT fluorescence excited by simultaneous absorption of two infrared photons from a pulsed laser with high peak power. We used an optical parametric amplifier (Spectra Physics OPA-800C) pumped by an amplified mode-locked Ti:sapphire laser with 130 fs pulses at a 1-kHz repetition rate. The excitation photon energy was tuned from 0.5 to 0.75 eV at a typical laser fluence of $\sim 5 \text{ J/m}^2$. In this regime, the fluorescence emission varied quadratically with laser intensity.¹² Fluorescence from the excited SWNT film surface was monitored using a liquid nitrogen cooled multichannel InGaAs detector (Jobin Yvon). To account for intensity

* Corresponding author. E-mail: gd2012@columbia.edu.

[†] Department of Chemistry.

[‡] Departments of Physics and Electrical Engineering.

[§] Current address: Department of Physics, University of California, Berkeley, CA 94720.

variation of excitation pulses at different excitation energies, we adopted an internal calibration scheme. Making use of the fact that the two-photon absorption is essentially flat when the two-photon energy is in the continuum states above the band gap,¹² the fluorescence spectra were normalized with lowest energy emission features where two-photon excitation energy is well within the plateau regime.

SWNTs have a definite symmetry with respect to a 180° rotation about an axis perpendicular to the nanotube through the center of a carbon hexagon.^{12,14} The excitonic states are either even (g) or odd (u) under this operation, and are labeled as 1g, 1u, 2g, 2u, etc.¹⁴ According to optical selection rules, the u-states are accessible by one-photon and the g-states by two-photon transitions. The dominant feature in the one-photon spectrum corresponds to a transition to the 1u state, which contains most of the oscillator strength.^{3,6,9} For two-photon transitions, one observes predominantly the 2g and the continuum states above the band gap.^{12,14} In this experiment, we investigate the exciton states associated with the E_{11} transitions, i.e., the transitions associated with the fundamental band gap of semiconducting nanotubes. A schematic energy scale for the exciton states is shown in Figure 1a. Two-photon excitation of 2g and continuum states is followed by fast relaxation into the 1u state, which then radiates by single-photon emission.

Figure 1b contains three representative fluorescence spectra excited at different two-photon energies. Several of peaks are observed in each spectrum; note that the onset of two-photon excitation is well above the 1u emission energy. This reflects the energy difference between the excited 2g state and the emitting 1u state. There are 22 different nanotube species, each uniquely defined by a set of indices (n,m), that fluoresce within the energy range shown in Figure 1b.¹⁸ While the emission peaks of smallest-diameter (largest transition energy) tubes are well separated in energy, at lower transition energies the emission features from different nanotube species overlap with each other. This makes the data analysis somewhat complicated.

To improve accuracy in determining the excitation profiles of individual peaks, we obtained difference fluorescence spectra by subtracting the fluorescence spectra excited by adjacent two-photon energies. The difference fluorescence spectra were fitted with multiple Lorentzian peaks with fixed position and width, corresponding to the individual nanotube species (see Figure 2a).¹⁸ When two or three nanotube species had emission peaks at similar energies, we used the published excitation spectra for HiPCO nanotubes to identify the structure with the dominant contribution.¹⁸ The difference excitation spectra were obtained by plotting the difference fluorescence intensity as a function of two-photon excitation energy. The difference excitation spectra were then integrated to obtain the two-photon excitation spectra, such as those shown in Figure 2b. Two-photon absorption arises mostly from the 2g exciton (the peak) and continuum states (the flat region).

The values of 1u–2g exciton energy splitting, $E_{2g} - E_{1u}$, for different nanotube species are listed in Table 1. We estimate the accuracy of these values to be around 10%. In

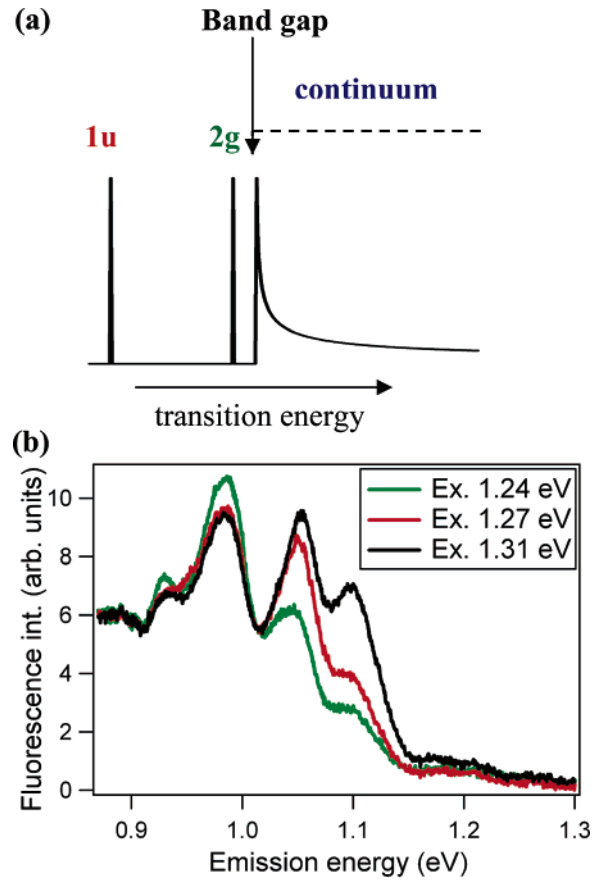


Figure 1. (a) Schematic representation of electronic transitions associated with the band gap in semiconducting SWNTs. The states below the band gap are bound excitons. One-photon absorption is allowed for the lowest-lying 1u state, while two-photon absorption is allowed for the 2g state. Absorption of two photons by the 2g and continuum states is followed by emission from the 1u state. (b) Representative normalized fluorescence spectra excited by two-photon energies of 1.24, 1.27, and 1.31 eV.

Figure 3a, we plot the value of $E_{2g} - E_{1u}$ as a function of inverse nanotube diameter ($1/d_t$). The data can be described by a proportional relation, with the points lying on a straight line of a slope ~ 0.24 eV·nm and zero y-intercept. Qualitatively, the fact that the nanotubes with smaller diameters have larger values of $E_{2g} - E_{1u}$, and therefore stronger excitonic effects, is not surprising, as the carriers are more confined in those nanotubes.^{6,10} Another way to state this is that the smaller-diameter nanotubes are closer to true one-dimensional structures.

A more quantitative understanding can be obtained by considering a model Hamiltonian representing the electron–hole interaction in a nanotube. Following the work of Perebeinos et al.,⁶ we can describe an exciton in a nanotube with diameter d_t by the Hamiltonian

$$H = -\frac{\hbar^2}{m_e} \frac{\partial^2}{\partial z^2} - \frac{e^2}{z} f\left(\frac{z}{\epsilon d_t}\right) \quad (1)$$

where z is the relative position of the electron and hole along the nanotube axis, ϵ is the effective dielectric constant, and m_e is the band mass of the electron.⁶ The Coulomb potential

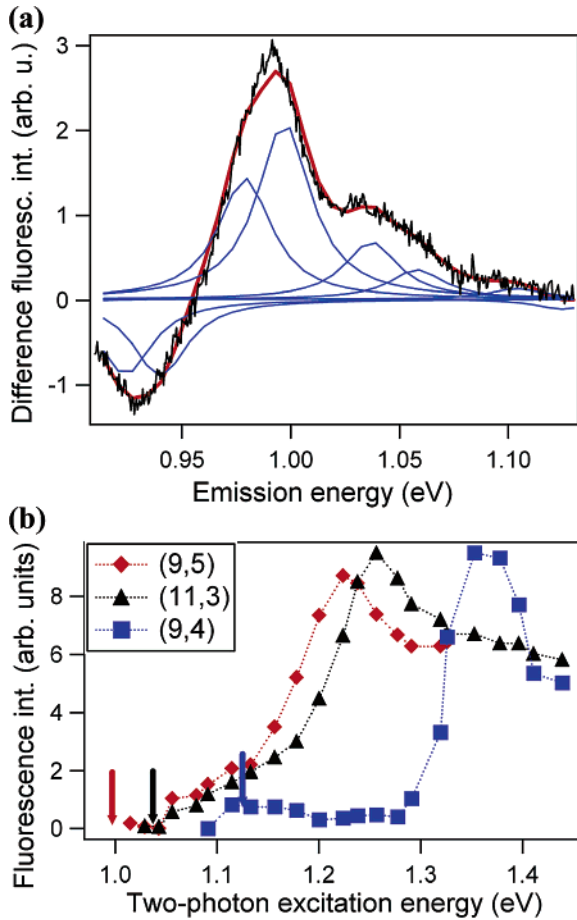


Figure 2. (a) Fitting procedure used to obtain two-photon excitation spectra of individual nanotube species. The difference fluorescence spectrum (black line) is obtained by subtracting the fluorescence excited with two-photon energy of 1.15 eV from the fluorescence spectrum excited with 1.21 eV. The difference fluorescence spectrum is fitted with Lorentzian peaks (blue lines) corresponding to the fluorescence contributions from individual nanotube species. The red line represents the sum of the Lorentzian contributions. (b) Two-photon excitation spectra for three different nanotube species. Energies of 1u excitons for each tube are shown with the solid arrows. Peaks correspond to the energies of 2g excitons. Two-photon absorption above the energy of the 2g peak is due to continuum transitions.

energy term includes a dimensionless function $f(z/\epsilon d_t)$ that accounts for both the quasi-one-dimensional nature of the nanotube and the variation of the effective dielectric constant with z . Despite the omission of chirality effects, it is a good approximation to take the electron band mass to vary inversely with the nanotube diameter: $m_e = \eta/d_t$, where η is a suitable constant of proportionality.¹ The Hamiltonian (1) can then be rewritten as

$$H = \frac{1}{d_t} \left[-\frac{\hbar^2}{\eta} \frac{\partial^2}{\partial^2 \zeta} - \frac{e^2}{\zeta} f\left(\frac{\zeta}{\epsilon}\right) \right] \quad (2)$$

where $\zeta \equiv z/d_t$ is the electron-hole separation in units of the nanotube diameter. Equation 2 shows that, within this model, the energy level structure of excitons will be identical for all nanotubes, with an overall inverse scaling with the nanotube diameter. Therefore, the ratio $(E_{\text{gap}} - E_{1u})/(E_{2g} -$

Table 1. Exciton Energy Levels and Structural Properties of the SWNTs Embedded in PMAOVE Matrix

E_{1u} (eV)	E_{2g} (eV)	$E_{\text{gap}} - E_{1u}$ (eV)	assignment ^a	d_t (nm)
1.30	1.60	0.42	(8,3)	0.78
1.26	1.57	0.43	(6,5)	0.76
1.21	1.49	0.39	(7,5)	0.83
1.18	1.42	0.34	(10,2)	0.88
1.13	1.37	0.34	(9,4)	0.91
1.10	1.35	0.35	(7,6)	0.89
1.06	1.31	0.35	(8,6)	0.96
1.04	1.26	0.31	(11,3)	1.01
1.00	1.23	0.33	(9,5)	0.97
0.98	1.18	0.29	(8,7)	1.03
0.94	1.16	0.30	(9,7)	1.10
0.92	1.12	0.27	(12,4)	1.14
0.89	1.08	0.27	(11,6)	1.18

^a From ref 18.

E_{1u}) will be the same for all semiconducting nanotube species. With this ratio we can determine the exciton binding energies from the values of $E_{2g} - E_{1u}$. Using a truncated Coulomb model potential, we determined this ratio to be 1.4 from the two-photon excitation spectra of small diameter tubes (such as (6,5)), for which the best excitation spectra could be recorded.¹² Similar results were reported recently using a cylindrical hydrogen model and ab initio calculations.¹⁴ Using the ratio of 1.4, it follows from our data that the binding energy of the 1u exciton relates to nanotube diameter as

$$E_{\text{gap}} - E_{1u} \cong \frac{0.34 \text{ eV}}{d_t} \quad (3)$$

where nanotube diameter is in nanometers.

The observed inverse proportionality of $E_{2g} - E_{1u}$ (and therefore the exciton binding energy) to nanotube diameter is consistent with the more general theory of Perebeinos et al.⁶ They describe the exciton binding energy in SWNTs by the relation $E_b \approx A d_t^{\alpha-2} m_e^{\alpha-1} \epsilon^{-\alpha}$, where A and α are constants.⁶ Within the approximation that the carrier effective mass varies inversely with the nanotube diameter,¹ we obtain $E_b \propto d_t^{-1} \epsilon^{-\alpha}$.

When the chirality dependence of carrier effective mass is included, this theory predicts a modification of the simple diameter dependence of the exciton binding energy.⁶ Specifically, it predicts increased exciton binding energies for nanotubes with $\text{mod}(n - m, 3) = 2$ ("mod 2") and reduced binding energies for $\text{mod}(n - m, 3) = 1$ ("mod 1") tubes of equal diameter. This would result in variation of several percent in binding energy for two tubes with the same diameter and different values of $\text{mod}(n - m, 3)$. Figure 3a shows that this effect is not observed in our data; it is apparently not detectable within our experimental accuracy.

Once we have determined the exciton binding energy, we can also estimate the energy of the band gap of each nanotube species by adding the values of E_{1u} to the binding energy of the 1u exciton. In Figure 3b, we plot the experimentally determined band-gap energy as a function of inverse nano-

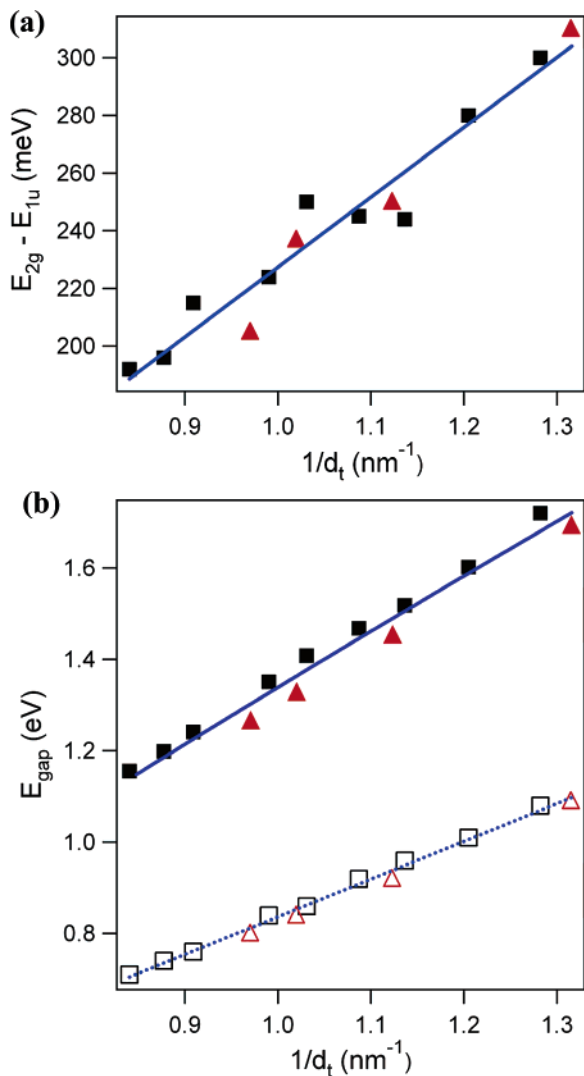


Figure 3. (a) Values of $E_{2g} - E_{1u}$ plotted as a function of inverse nanotube diameter. The solid line best describes the relationship between $E_{2g} - E_{1u}$ and $1/d_t$. Different trends in values of $E_{2g} - E_{1u}$ for “mod 1” (red triangles) and “mod 2” (black squares) tubes are not observed. (b) Comparison of the measured band-gap energies (solid symbols) with those predicted by tight-binding theory (open symbols).¹ Solid blue line corresponds to eq 4 in text. The dashed blue line is the linear fit to the tight-binding values ($E_{gap} = (0.84 \text{ eV})/d_t$). In the tight-binding calculations, we used $\gamma = 2.9 \text{ eV}$. For both measured and tight-binding values, E_{gap} is consistently lower for “mod 1” (red triangles) than the “mod 2” tubes (black squares) of similar diameter.

tube diameter. The results are well described by the equation

$$E_{gap} = \frac{0.34 \text{ eV}}{d_t} + \frac{1.11 \text{ eV}}{d_t + 0.11} \quad (4)$$

where nanotube diameter is in nanometers. The first term corresponds to scaling of the exciton binding energy with nanotube diameter (eq 3). The coefficients in the second term were determined by the best fit to the data. This term describes the scaling of E_{1u} and is similar to the dominant term in the published relationship of fluorescence energy and diameter.¹⁸

In Figure 3b, the experimental values for E_{gap} are compared with the values predicted by tight-binding theory.¹ The

experimental band gap values are about 1.6 times higher than those predicted. The ratio is approximately constant, as both values have a predominant dependence on inverse diameter. Note, however, that values of band gap lie slightly below the straight line for “mod 1” and above for the “mod 2” nanotubes for both measured and tight-binding values. This is not surprising, as the pattern in the experimental values of E_{gap} is determined predominately by the values of E_{1u} , which show this “mod” dependence.¹⁸ The measured values of E_{1u} are assigned to specific nanotube structures by comparing them to the pattern expected from tight-binding theory.¹⁸ The significant difference between the measured and tight-binding values of E_{gap} directly illustrates the importance of many-body effects in SWNTs.

It is also useful to compare the measured trend in band-gap energies to a calculation that includes many-body effects in computation of the band-gap energy. Spataru et al. have made such calculations for SWNTs with small diameters.⁹ They predicted that the (8,0) nanotube with diameter of 0.63 nm should have a $\sim 2.5 \text{ eV}$ band gap corresponding to the optically active states (in air).⁹ Our experimental trend predicts the band-gap energy to be approximately 2.0 eV. Some of the discrepancy between the two values could be explained by the difference in dielectric environment.

It is important to remember that we measured exciton binding and band-gap energies for SWNTs inside a polymer matrix, where electron–hole interactions are subject to external dielectric screening. Many-body effects should be even more pronounced for a SWNT in vacuum or air, where the dielectric screening due to the environment is absent. We therefore expect the exciton binding energies for nanotubes in air to be somewhat higher than the measured values reported above. The fluorescence energies (E_{1u}) also depend on nanotube environment.^{19–22} For SWNTs suspended in air the values of E_{1u} are $\sim 30 \text{ meV}$ higher than the fluorescence energies of SWNTs in SDS solution.²² Another 20–30 meV blue shift in transition energy is observed when the air-suspended tubes are heated.^{23,24} The expected increased exciton binding energy and the measured blue shift of E_{1u} in air-suspended tubes should result in higher E_{gap} values than those measured for SWNTs inside a polymer matrix.

In summary, we have used two-photon excitation spectroscopy to measure the exciton energies for a range of individual semiconducting nanotube species. This allowed us to determine how the exciton binding and band-gap energies vary with nanotube structure. We found that both quantities scale inversely with nanotube diameter. Both the large exciton binding energy and the increased band-gap energy are expressions of the many-body effects that dominate the electronic properties of semiconducting SWNTs.

Acknowledgment. We thank V. Perebeinos, M. Hybertsen, and C. Spataru for insightful discussions, Y. Rao and M. Comstock for experimental support, and R. Smalley for a generous gift of as-grown HiPCO nanotubes. Financial support was provided by Nanoscale Science and Engineering Initiative of the NSF (CHE-0117752), by the New York State Office of Science, Technology, and Academic Research

(NYSTAR), and by the Office of Basic Energy Sciences, US Department of Energy (DOE-FG02-98ER14861 and DE-FG02-03ER15463).

References

- (1) Saito, R.; Dresselhaus, G.; Dresselhaus, M. S. *Physical properties of carbon nanotubes*; Imperial College Press: London, 1998.
- (2) Ogawa, T. In *Optical properties of low-dimensional materials*; Ogawa, T., Kanemitsu, Y., Eds.; World Scientific Publishing Co. Pte Ltd: Singapore, 1995.
- (3) Ando, T. *J. Phys. Soc. Jpn.* **1997**, *66*, 1066–1073.
- (4) Kane, C. L.; Mele, E. J. *Phys. Rev. Lett.* **2003**, *90*, 207401.
- (5) Ichida, M.; Mizuno, S.; Saito, Y.; Kataura, H.; Achiba, Y.; Nakamura, A. *Phys. Rev. B* **2002**, *65*, 241407.
- (6) Perebeinos, V.; Tersoff, J.; Avouris, P. *Phys. Rev. Lett.* **2004**, *92*, 257402.
- (7) Zhao, H. B.; Mazumdar, S. *Phys. Rev. Lett.* **2004**, *93*, 157402.
- (8) Chang, E.; Bussi, G.; Ruini, A.; Molinari, E. *Phys. Rev. Lett.* **2004**, *92*, 196401.
- (9) Spataru, C. D.; Ismail-Beigi, S.; Benedict, L. X.; Louie, S. G. *Phys. Rev. Lett.* **2004**, *92*, 077402.
- (10) Pedersen, T. G. *Phys. Rev. B* **2003**, *67*, 073401.
- (11) Htoon, H.; O'Connell, M. J.; Cox, P. J.; Doorn, S. K.; Klimov, V. I. *Phys. Rev. Lett.* **2004**, *93*, 027401.
- (12) Wang, F.; Dukovic, G.; Brus, L. E.; Heinz, T. F. *Science* **2005**, *308*, 838–841.
- (13) Ma, Y.-Z.; Valkunas, L.; Bachilo, S. M.; Fleming, G. R. *J. Phys. Chem. B* **2005**, *109*, 15671–15674.
- (14) Maultzsch, J.; Pomraenke, R.; Reich, S.; Chang, E.; Prezzi, D.; Ruini, A.; Molinari, E.; Strano, M. S.; Thomsen, C.; Lienau, C. *Los Alamos National Laboratory, Preprint Archive, Condensed Matter* **2005**, arXiv: cond-mat/0505150.
- (15) Nikolaev, P.; Bronikowski, M. J.; Bradley, R. K.; Rohmund, F.; Colbert, D. T.; Smith, K. A.; Smalley, R. E. *Chem. Phys. Lett.* **1999**, *313*, 91–97.
- (16) As-grown HiPCO nanotubes from Carbon Nanotechnologies Inc., Houston, TX.
- (17) Dukovic, G.; White, B. E.; Zhou, Z. Y.; Wang, F.; Jockusch, S.; Steigerwald, M. L.; Heinz, T. F.; Friesner, R. A.; Turro, N. J.; Brus, L. E. *J. Am. Chem. Soc.* **2004**, *126*, 15269–15276.
- (18) Bachilo, S. M.; Strano, M. S.; Kittrell, C.; Hauge, R. H.; Smalley, R. E.; Weisman, R. B. *Science* **2002**, *298*, 2361–2366.
- (19) Moore, V. C.; Strano, M. S.; Haroz, E. H.; Hauge, R. H.; Smalley, R. E.; Schmidt, J.; Talmon, Y. *Nano Lett.* **2003**, *3*, 1379–1382.
- (20) Hertel, T.; Hagen, A.; Talalaev, V.; Arnold, K.; Hennrich, F.; Kappes, M.; Rosenthal, S.; McBride, J.; Ulbricht, H.; Flahaut, E. *Nano Lett.* **2005**, *5*, 511–514.
- (21) Hartschuh, A.; Pedrosa, H. N.; Novotny, L.; Krauss, T. D. *Science* **2003**, *301*, 1354–1356.
- (22) Lefebvre, J.; Fraser, J. M.; Homma, Y.; Finnie, P. *Appl. Phys. A* **2004**, *78*, 1107–1110.
- (23) Finnie, P.; Homma, Y.; Lefebvre, J. *Phys. Rev. Lett.* **2005**, *94*, art. no. 247401.
- (24) Milkie, D. E.; Staii, C.; Paulson, S.; Hindman, E.; Johnson, A. T.; Kikkawa, J. M. *Nano Lett.* **2005**, *5*, 1135–1138.

NL0518122